Prediction of Welding Thermal History by a Comprehensive Solution

Thermal histories, cooling times and shapes of heat-affected zones can be predicted by a comprehensive heat conduction solution

BY T. KASUYA AND N. YURIOKA

ABSTRACT. A comprehensive solution has been developed to examine heat conduction in three different welding cases. Case I is a quasi-steady-state model to predict the shape of the heat-affected zone (HAZ), and the thermal histories and cooling times between 800° and 500°C ($t_{8/5}$) in wide plates. Case II is an instantaneous heat source model to predict cooling time from solidification to 100°C (t_{100}) in small test pieces. Case III is an unsteady heat model to predict t_{100}s in locally preheated plates. Rosenthal's and Tanaka's formulas can be derived from a solution of Case I. These three cases were applied to the predictions of thermal histories, cooling times and HAZ shapes. The calculated results have been compared with the experimental results of several different cases of arc welding and good agreement has resulted.

Introduction

Since mechanical properties of welds such as hardness and toughness are greatly affected by welding thermal history, a number of researchers (Refs. 1–18) have reported on thermal history prediction and its application to the estimation of welded joint qualities. Rosenthal (Refs. 1, 2) derived an analytical solution for a welding heat flow problem under the assumption that a point heat source is on the plate surface and that there is no surface heat transfer. His solution has been used worldwide to predict welding thermal history and cooling rates.

Tanaka (Ref. 3) solved welding heat flow without neglecting surface heat transfer. Owing to surface heat transfer, Tanaka's solution is more complicated than Rosenthal's. However, surface heat transfer must be taken into account in welding heat conduction because it varies from welding process to process; it is very low in submerged arc welding, due to covering flux, and is very high in electroslag and electrogas welding, due to water cooling. Tanaka also proved that Rosenthal's solution is a special case of his solution.

In the case of high heat input welding, the assumption of a surface point heat source is not valid. A heat source in this case is considered to expand beneath the plate surface. In order to analyze heat flow in high heat input welding, it is necessary to derive a solution under the condition that a point heat source is located inside a plate and that heat of varying extent flows at the surface.

Rosenthal and Tanaka solved a heat flow problem of a quasi-steady state. When a plate to be welded is wide enough, heat flow approaches the quasi-steady state. This is the case with most welding. When welding test pieces for cold cracking or HAZ hardness, thermal history is influenced by the test piece size and the weld bead length. Cold cracking or hydrogen-assisted cracking can be avoided by the employment of preheating, which reduces the cooling rate, especially around 200°C (392°F), to facilitate the evolution of hydrogen from a weld. Therefore, cooling time from solidification to 100°C (212°F), t_{100}, is a thermal parameter by which the hydrogen evolution is assessed. The derivation of a solution of heat flow in a small test piece is needed to determine the necessary preheating temperature from the results of cold cracking tests. This is done by comparing cooling times of welding a small test piece with those of actual welding.

Weldability test specimens are generally preheated uniformly. However, weldments in actual welding are often preheated along a welding line only, *i.e.*, local preheating is performed. Welding cooling times differ, sometimes significantly, from local preheating to uniform preheating.

The purpose of the present study is to present analytical solutions for thermal history in wide plate welding, small test piece welding and locally preheated welding.

KEY WORDS

Thermal History
Cooling Rates
HAZ Shape
Heat Conduction
Analytical Model
Heat Flow
Surface Heat Transfer
Point Heat Source
High Heat Input Weld
Weld Cooling Time

Heat Conduction Models and Their Solutions

Models of Heat Flow in Welding

Constant thermal properties are assumed in the present study. Thus, the following heat conduction equation holds in this case:

$$\frac{\partial T}{\partial T} = \kappa \nabla^2 T \left(\nabla^2 = \frac{\partial^2}{\partial x^2} + \frac{\partial^2}{\partial y^2} + \frac{\partial^2}{\partial z^2} \right) \quad (1)$$

where κ is thermal diffusivity (mm^2/s).

T. KASUYA and N. YURIOKA are with the Joining Technical Development Bureau, Nippon Steel Corp., Chiba-ken, Japan.

Paper presented at the 72nd Annual AWS Meeting, held April 15–19, 1991, Detroit, Mich.

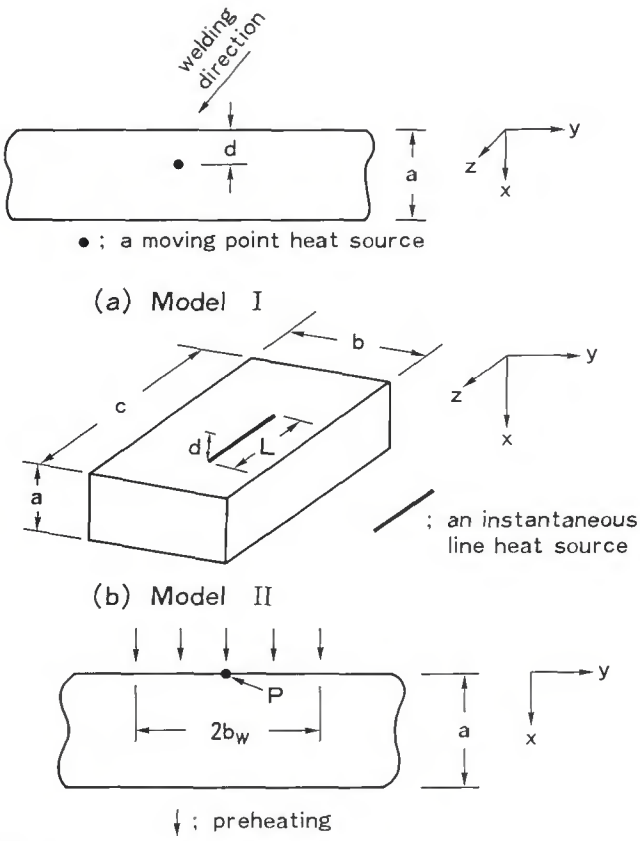

Fig. 1 — Models of welding heat flow problem.

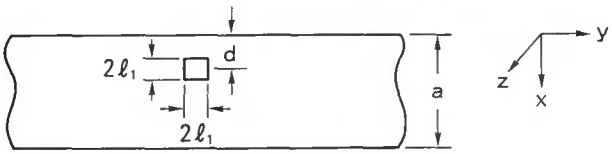

Fig. 2 — A first step for Model I. A small cubic instantaneous heat is added when t = 0.

Surface heat transfer is assumed to obey Newton's cooling law, and thus the boundary condition becomes

$$\lambda \frac{\partial T}{\partial n} = -\alpha (T - T_\infty)$$

where n is normal coordinate to the surface, λ is thermal conductance (J/°C mms) and α is surface heat transfer coefficient (J/°C mm^{2}s). This study introduces three different types of heat flow models.

Model I: A Quasi-Steady-State Model for Wide Plates

In most actual welding, a plate to be welded is regarded as infinitely wide and long from the viewpoint of heat flow due to a concentrated heat source in welding. Model I is a point heat source moving inside a plate as seen in Fig. 1A, under a quasi-steady-state condition during the whole welding time, except the very beginning and end of welding. The heat flow due to an expanded heat source encountered in high heat input welding can be investigated by distributing a point heat source of Model I inside a plate.

Model II: An Instantaneous Line Heat Model for Small Test Pieces

The thermal history in small test piece welding is influenced by the test piece size and the weld bead length. In this case, a quasi-steady state of heat flow cannot be attained during the whole welding period. Furthermore, the cooling time to low temperatures, such as t_{100}, is not influenced significantly by the shape of the welding heat source as long as the same energy is supplied as the total welding heat input. It follows that an instantaneous line heat model, as shown in Fig. 1B, has been introduced.

Model III: A Model for Locally Preheated Plates

When local preheating is conducted, the temperature distribution in a plate is already nonuniform at the start of welding. Therefore, the model shown in Fig. 1C is introduced to analyze the heat flow of local preheating. The temperature distribution depends on the power of preheat, q_h (J/mm^{2}s), and its width, $2b_w$ (mm).

Analytical Solution

To solve Equations 1 and 2, temperature, θ, (= T − T_∞) is expressed as follows:

$$\theta = X(x)Y(y)Z(z)\Psi(t) \qquad (3)$$

In the coordinate system shown in Fig. 1, the functions on the right-hand side of Equation 3 are given by substituting Equation 3 into Equation 1, as follows:

$$X = A_x \sin\left(\frac{ux}{a}\right) + B_x \cos\left(\frac{ux}{a}\right)$$
$$Y = A_y \sin(vy) + B_y \cos(vy)$$
$$Z = A_z \sin(wz) + B_z \cos(wz)$$
$$\Psi = \exp\left\{-\left(\frac{u^2}{a^2} + v^2 + w^2\right)\kappa t\right\} \qquad (4)$$

where u, v and w are values to be determined by the boundary condition. Equation 3 must satisfy the boundary condition of Equation 2. Thus,

$$l\frac{\partial X}{\partial x} = -aX,(x = a);\ l\frac{\partial X}{\partial x} = aX,(x = 0) \qquad (5)$$

where a is thickness of a welded plate (mm).

Therefore, X is given as follows:

$$X = A_n \left\{ \begin{array}{l} \cos\left(\frac{u_n x}{a}\right) + \\ B_i \sin\left(\frac{u_n x}{a}\right) / u_n \end{array} \right\}$$

u_n: n − th root (characteristic value)

$$of\ \tan(u_n) = \frac{2B_i u_n}{(u_n^2 - B_i^2)} \qquad (6)$$

where B_i is a dimensionless Biot modulus (= $a\alpha/\lambda$).

A_n in Equation 6 is given by the initial condition. The symmetry of heat flow gives the coefficients as:

$$A_y = A_z = 0 \qquad (7)$$

B_y and B_z are also given by the initial condition. Let us suppose that f(x), $g_1(y)$ and $g_2(z)$ are arbitrary functions of x, y and z coordinates, respectively. If the temperature distribution at the start of

welding is assumed as a function, $f(x)g_1(y)g_2(z)$, the following relations are given:

$$A_n = \frac{2u_n^2}{(u_n^2 + B_i^2)a + 2B_i a} \int_o^a \left\{ cos\left(\frac{u_n}{a}x\right) + \frac{B_i}{u_n} sin\left(\frac{u_n}{a}x\right) \right\} f(x)dx \quad (8a)$$

$$\int_{-\infty}^{\infty} B_y(v)cos(vy)dv = g_1(y) \quad (8b)$$

$$\int_{-\infty}^{\infty} B_z(w)cos(wz)dw = g_2(z) \quad (8c)$$

Equation 8 is valid only when a body is infinite in the y and z directions. In the case of a small test piece, B_y and B_z must be given in a form of Equation 8a.

Equation 3, along with Equations 6, 7 and 8, is the comprehensive solution for the analyses of heat flow in Models I, II and III. This solution has been applied to Models I, II and III, as shown below.

Model I

From Equation 8, relative temperature, θ , is given as follows:

$$\theta = \sum_{n=1}^{\infty} A_n \left\{ cos\left(\frac{u_n}{a}x\right) + \frac{B_i}{u_n} sin\left(\frac{u_n}{a}x\right) \right\} exp\left(-\kappa t \frac{u_n^2}{a^2}\right) x \int_{-\infty}^{\infty} B_y(v)cos(vy) exp(-\kappa t v^2)dv \cdot \int_{-\infty}^{\infty} B_z(w)cos(wz) exp(-\kappa t w^2)dw \quad (9)$$

Assuming a small cubic instantaneous heat, an instantaneous heat source, Q (J) is given at x = d, y = 0 and z = 0 when t =0 and the cubic heat source with a length of $2\ell_1$ is d (mm) under the surface, as shown in Fig. 2, the initial condition becomes

$$\theta = Q/\rho c_p(2\ell_1)^3,$$
$$d - \ell_1 < x < d + \ell_1;$$
$$-\ell_1 < y < \ell_1 - \ell_1 < z < \ell_1$$
$$\theta = 0, \ \textit{the other region} \quad (10a)$$

where ρ is density (kg/mm^3) and c_p is specific heat (J/kg°C).

The initial condition of Equation 10a can be rewritten by using f(x), $g_1(y)$ and $g_2(z)$ as follows:

$$\theta = f(x)g_1(y)g_2(z)$$
$$f(x) = \begin{cases} Q/\rho c_p(2\ell_1), \\ d - \ell_1 < x < d + \ell_1 \\ 0, \ \textit{the other region} \end{cases}$$

$$g_1(y) = \begin{cases} \frac{1}{2}\ell_1, \\ -\ell_1 < y < \ell_1 \\ 0, \ \textit{the other region} \end{cases}$$

$$g_2(z) = \begin{cases} \frac{1}{2}\ell_1, \\ -\ell_1 < z < \ell_1 \\ 0, \ \textit{the other region} \end{cases} \quad (10b)$$

Substituting Equation 10b into Equations 8a, 8b and 8c, the coefficients in Equation 9 are given as follows:

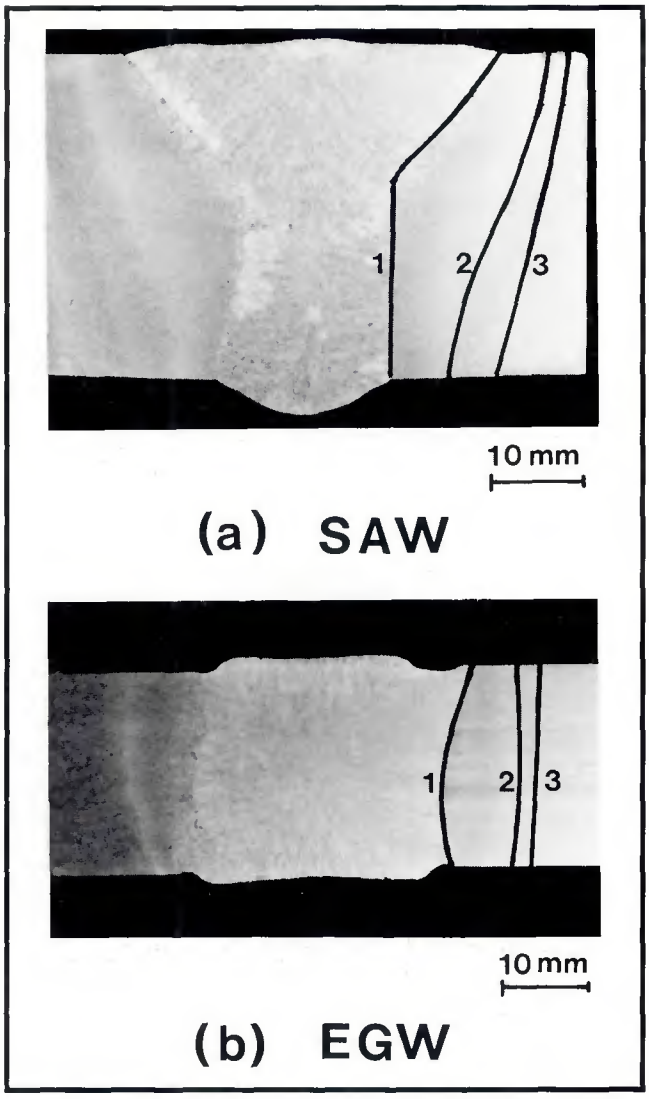

Fig. 3 — Macro specimens of SAW and EGW: 1) weld interface; 2) A_{c3}; and 3) A_{c1}). The welding conditions are shown in Table 1.

Table 1 — Welding Conditions of SAW, EGW and SMAW

Welding Method		Current (A)	Voltage (V)	Speed (mm/s)	Heat Input (kJ/mm)	Thickness (mm)	Water Coolant Rate (L/s)
SAW	L	1450	38	6.33	24.6	35	—
	T1	1200	42				
	T2	1050	48				
EGW		640	37	1.22	19.4	25	0.05
SMAW		120	24	3.58	0.8	9, 16, 20	—
		170	25	2.5	1.7	9, 16, 20	
		285	29	1.83	4.5	9, 16, 20	

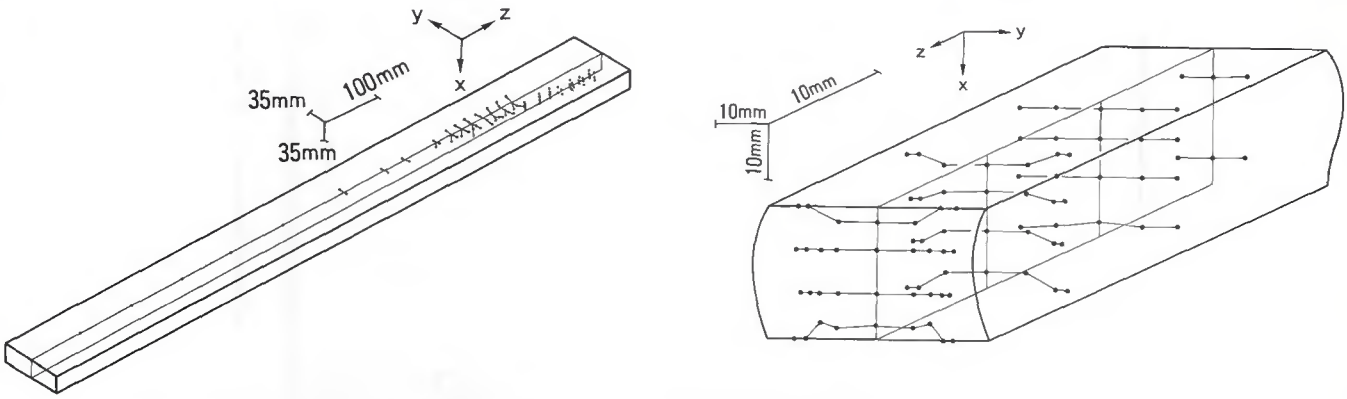

Fig. 4 — Groups of point heat sources for simulating thermal histories and predicting HAZ shapes with SAW and EGW.

$$A_n = \frac{2Qu_n}{\left\{\left(u_n^2 + B_i^2\right) + 2B_i\right\}\ell_1 \rho c_p} \sin\left(\frac{u_n}{a}\ell_1\right) \left\{\cos\left(\frac{u_n}{a}d\right) + \frac{B_i}{u_n}\sin\left(\frac{u_n}{a}d\right)\right\}$$

$$B_y(v) = \frac{1}{2\pi\ell_1 v}\sin(v\ell_1)$$

$$B_z(w) = \frac{1}{2\pi\ell_1 w}\sin(w\ell_1) \qquad (11)$$

A solution for a point heat source is given by reducing ℓ_1 to zero

$$\theta = \frac{Q}{2\pi a\lambda t}\sum_{n=1}^{\infty} A_n \left\{\cos\left(\frac{u_n}{a}x\right) + \frac{B_i}{u_n}\sin\left(\frac{u_n}{a}x\right)\right\} \exp\left(-\frac{y^2+z^2}{4\kappa t} - \kappa\frac{u_n^2}{a^2}t\right) \qquad (12)$$

where $A_n =$

$$\frac{u_n^2}{u_n^2 + B_i^2 + 2B_i}\left\{\cos\left(\frac{u_n}{a}d\right) + \frac{B_i}{u_n}\sin\left(\frac{u_n}{a}d\right)\right\}$$

Suppose that a point heat source starts at $t = -\tau_0$ and that its z coordinate at t = 0 is zero. In the light of Equation 12, a solution at $t = \tau$ for a point heat source moving at constant velocity of v_s (mm/s) can be obtained by integrating θ with respect to t from $-\tau_0$ to τ. This kind of solution is valid because the linearity in temperature holds in the heat conduction equation of Equation 1, and the boundary condition of Equation 2. Thus, θ is given by the summation of the temperature increment caused by point heats from $t = -\tau_0$ to $t = \tau$. When total heat input, Q (J) is considered to be heat input given at the time interval, dt, then Q is expressed as qdt, where q is welding heat input (J/s). In this case, θ in Equation 12 can be considered as the temperature increment, $d\theta$, and temperature, θ at $t = \tau$ is given as follows:

$$\theta = \frac{q}{2\pi a\lambda}\sum_{n=1}^{\infty} A_n \left\{\cos\left(\frac{u_n}{a}x\right) + \frac{B_i}{u_n}\sin\left(\frac{u_n}{a}x\right)\right\} \times \int_{-\tau_0}^{\tau} \exp\left(-\frac{u_n^2}{a^2}\kappa(\tau - t) - \frac{y^2 + (z - v_s t)^2}{4\kappa(\tau - t)}\right)\frac{dt}{\tau - t} \qquad (13)$$

When heat flow is in a steady state, τ_0 must be infinite, thus, Equation 13 becomes

$$\theta = \frac{q}{\pi a\lambda}\sum_{n=1}^{\infty} A_n \left\{\cos\left(\frac{u_n}{a}x\right) + \frac{B_i}{u_n}\sin\left(\frac{u_n}{a}x\right)\right\} \exp\left(-\frac{v_s(z - v_s t)}{2\kappa}\right) K_0 \left\{r\sqrt{\frac{u_n^2}{a^2} + \frac{v_s^2}{4\kappa^2}}\right\} \qquad (14)$$

where, A_n is given in Equation 12 and K_0 is 0 order modified Bessel function of the second kind, and r is $\sqrt{y^2 + (z - v_s t)^2}$. In Equation 14, τ has been replaced with t. When d is zero, A_n is $u_n^2/(u_n^2 + B_i^2 + 2B_i)$, *i.e.*, Equation 14 becomes Tanaka's solution of a surface point heat source.

Model II

A solution for Model II is used to predict welding cooling times of a small test piece. From Equation 6, the solution for this case is as follows:

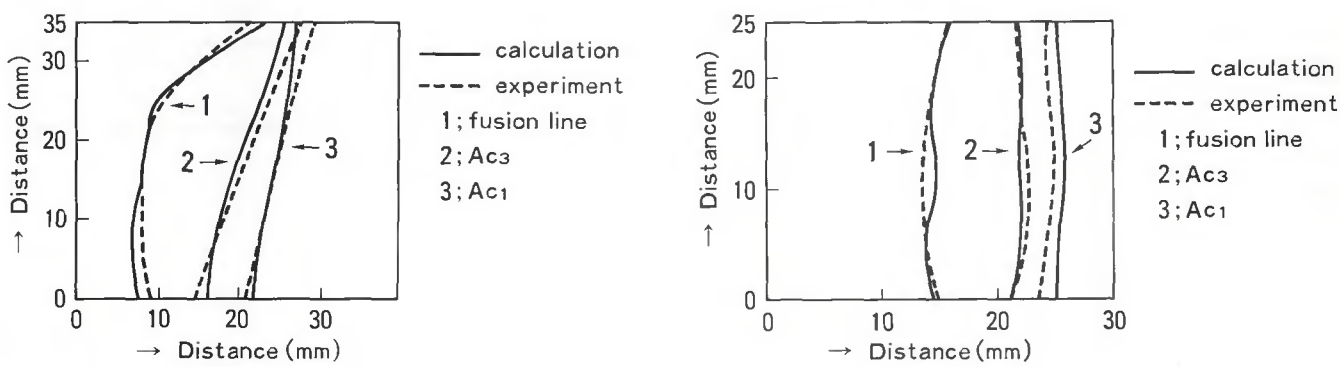

Fig. 5 — Results of HAZ simulations of SAW and EGW using the groups of point heat sources shown in Fig. 4. The thermal properties used are shown in Table 2.

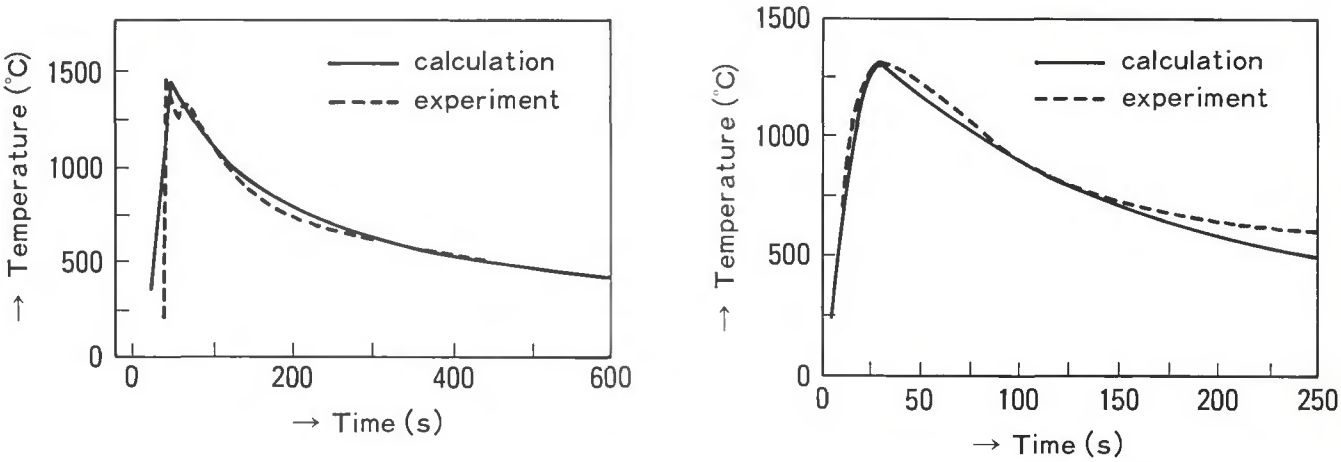

Fig. 6 — Thermal histories of SAW and EGW using the groups of point heat sources shown in Fig. 4. The thermal properties used are shown in Table 2.

$$\theta = \sum_{n=1}^{\infty} A_n \left\{ cos\left(\frac{u_n}{a}x\right) + \frac{B_i}{u_n} sin\left(\frac{u_n}{a}x\right) \right\}$$
$$exp\left(-\kappa t \frac{u_n^2}{a^2}\right)$$
$$x \sum_{m=1}^{\infty} B_m \left\{ cos\left(\frac{v_m}{b}y\right) + \frac{B_b}{v_m} sin\left(\frac{v_m}{b}y\right) \right\}$$
$$exp\left(-\kappa t \frac{v_m^2}{b^2}\right)$$
$$x \sum_{s=1}^{\infty} C_s \left\{ cos\left(\frac{w_s}{c}z\right) + \frac{B_c}{w_s} sin\left(\frac{w_s}{c}z\right) \right\}$$
$$exp\left(-\kappa t \frac{w_s^2}{c^2}\right)$$
$$u_n : n-th\ root\ of\ tan(u_n) = 2B_i u_n / (u_n^2 - B_i^2)$$
$$v_m : m-th\ root\ of\ tan(v_m) = 2B_b v_m / (v_m^2 - B_b^2)$$
$$w_s : s-th\ root\ of\ tan(w_s) = 2B_c w_s / (w_s^2 - B_c^2) \qquad (15)$$

where B_b (= $b\alpha/\lambda$) and B_c (= $c\alpha/\lambda$) are Biot moduli.

The coefficients, A_n, B_m and C_s in Equation 15 must be determined for an instantaneous line heat source and uniform preheating. First, the line heat with a length of 2L has been considered. When the edge length of its cross-section is $2l_2$, the initial condition becomes

$$\theta = Q_L / (8\rho c_p \ell_2^2 L)$$
$$d - \ell_2 < x < d + \ell_2;$$
$$b/2 - \ell_2 < y < b/2 + \ell_2;$$
$$c/2 - L < z < c/2 + L$$
$$\theta = 0,\ the\ other\ region \qquad (16)$$

Table 2 — Thermal Properties Used in This Study

Welding Method	Figs.	λ Thermal Conductance (J/°Cmms)	κ Thermal Diffusivity (mm²/s)	α Surface Heat Transfer Coefficient (J/°Cmm²s) (×10⁻⁵)	η Efficiency
SAW	5A, 6A, 7	0.0376	4.1	1.09	1.0
EGW	5B, 6B	0.0309	4.2	15.5	0.8
SMAW	8A, 8B	see Eq. 26	see Eq. 27	7.52	0.8
SMAW	9, 10	0.0543	12.0	2.09	0.8
—	11, 12	0.0543	12.0	2.09	—

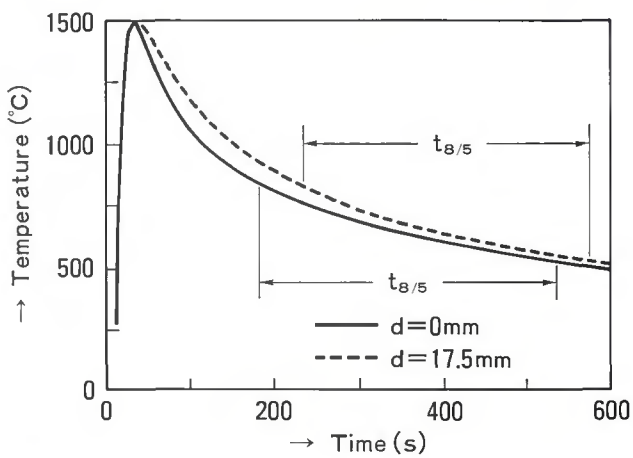

Fig. 7 — Effect of the location of a point heat source on thermal history (SAW). The welding condition and thermal properties used are shown in Tables 1 and 2, respectively.

The initial condition of Equation 16 can be rewritten by using f(x), $g_1(y)$ and $g_2(z)$ in the same fashion as Equation 10b. Hence, when ℓ_2 becomes zero, A_n, B_m and C_s are given from Equation 16 and Equation 8a as follows:

$$A_n = \frac{Q_L}{\rho c_p a} \cdot \frac{2u_n^2}{u_n^2 + B_i^2 + 2B_i} \left\{ cos\left(\frac{u_n}{a}d\right) + \frac{B_i}{u_n} sin\left(\frac{u_n}{a}d\right) \right\}$$

$$B_m = \frac{1}{b} \cdot \frac{2v_m^2}{v_m^2 + B_b^2 + 2B_b} \left\{ cos\left(\frac{v_m}{2}\right) + \frac{B_b}{v_m} sin\left(\frac{v_m}{2}\right) \right\}$$

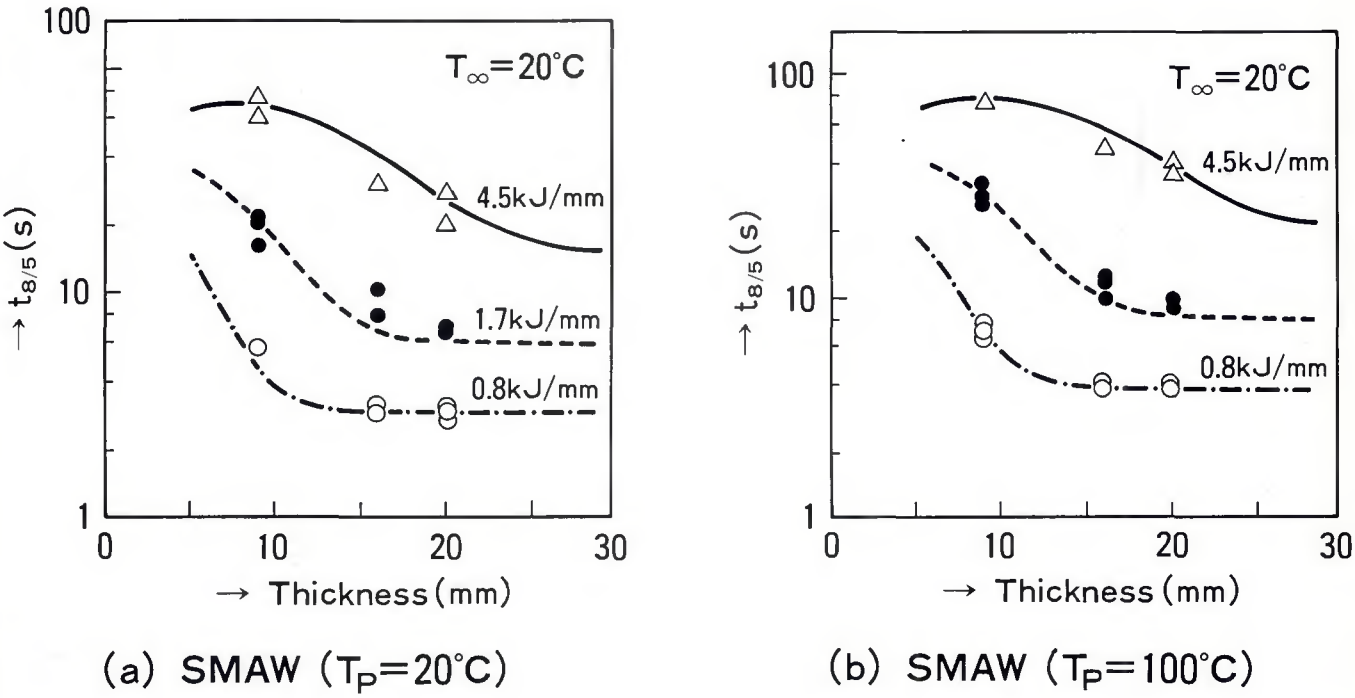

Fig. 8 — $t_{8/5}$s of experiments and calculations. The welding conditions and the thermal properties used are shown in Tables 1 and 2, respectively.

$$C_s = \frac{1}{L}\cdot\frac{2w_s}{w_s^2+B_c^2+2B_c}\sin\left(\frac{w_s}{c}L\right)\cdot\left\{\cos\left(\frac{w_s}{2}\right)+\frac{B_c}{w_s}\sin\left(\frac{w_s}{2}\right)\right\} \quad (17)$$

Second, a uniform preheating case is considered. This initial condition for uniform preheating is as follows:

$$\theta = T_p - T_\infty\begin{pmatrix}0<x<a,\ 0<y\\ <b,\ 0<z<c\end{pmatrix} \quad (18)$$

The initial condition of Equation 18 can be also rewritten by using f(x), $g_1(y)$ and $g_2(z)$ in the same fashion as Equation 10b. In most welding cases, B_i, B_b and B_c are order of 0.1 and thus B_i, B_b, $B_c < \pi/2$. Therefore, A_n, B_m and C_s become from Equation 8a as follows:

$$A_n = \frac{2B_i(T_p-T_\infty)}{u_n^2+B_i^2+2B_i}\left\{1+(-1)^{n+1}\right\}$$

$$B_m = \frac{2B_b}{v_m^2+B_b^2+2B_b}\left\{1+(-1)^{m+1}\right\}$$

$$C_s = \frac{2B_c}{w_s^2+B_c^2+2B_c}\left\{1+(-1)^{s+1}\right\} \quad (19)$$

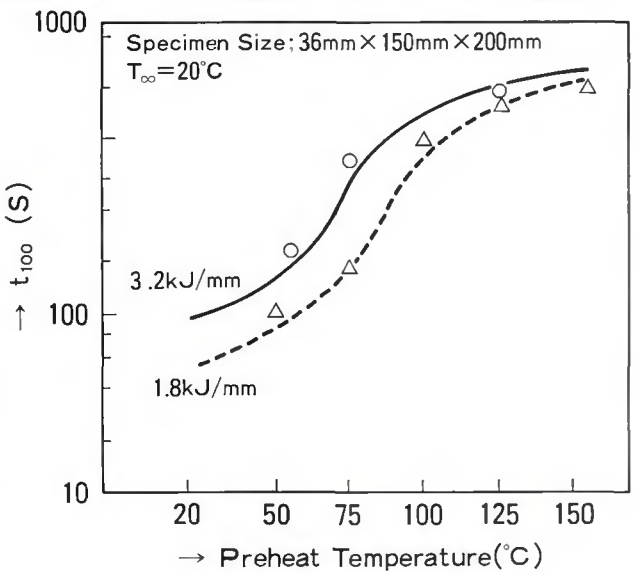

Fig. 9 — Comparison of calculated and experimental t_{100}s. The welding conditions and thermal properties used are shown in Tables 1 and 2, respectively.

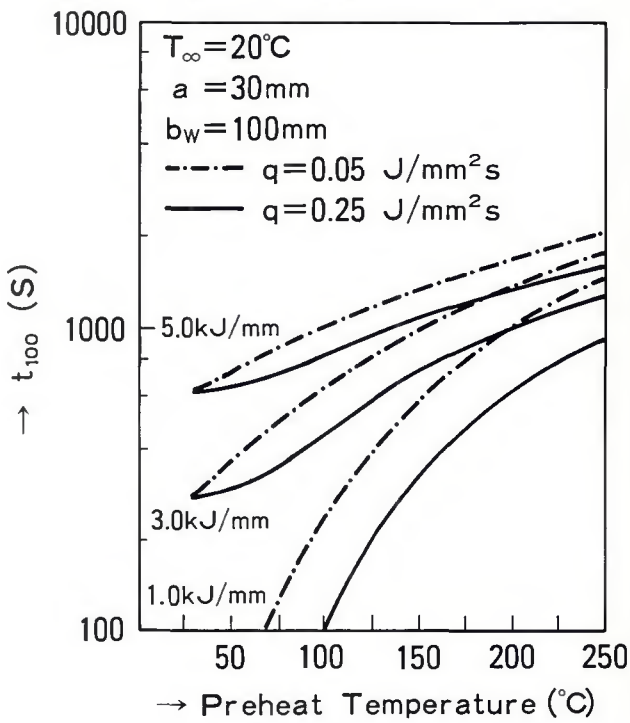

Fig. 10 — t_{100} calculation of actual welding by the linear combination of Model I and Model III. The thermal properties used are shown in Table 2.

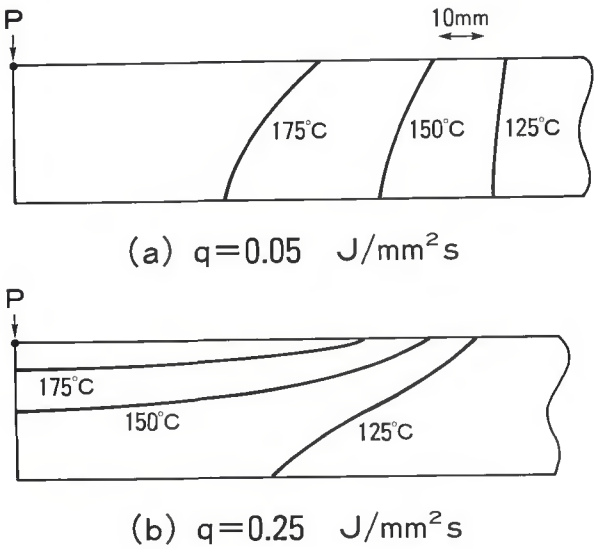

Fig. 11 — Temperature distribution at preheat temperature = 200°C (b_w, half width of preheating, = 100 mm) calculated by Model III. The thermal properties used are shown in Table 2.

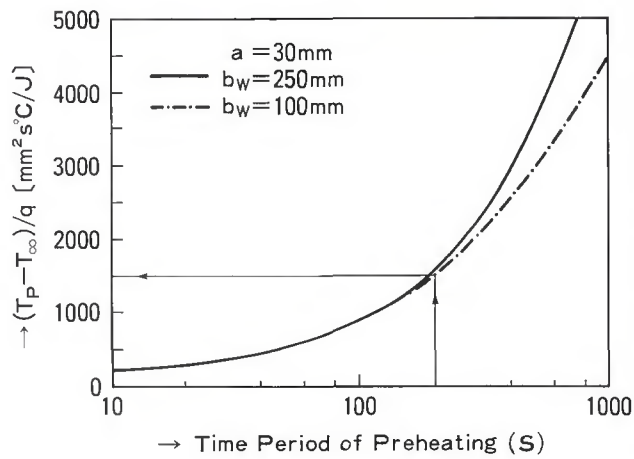

Fig. 12 — Chart to estimate preheat power, q_h (J/mm²s). The lines show temperature increases at the center of preheating which are calculated by Model III. The thermal properties used are shown in Table 2.

When a uniformly preheated test piece is welded, cooling times such as t_{100} can be calculated by the linear combination of Equation 15 along with Equations 17 and 19.

Model III

Model III is a two-dimensional (x and y direction) heat flow problem of locally preheated plates. In light of Equation 6, the solution for this case is as follows:

$$\theta = \sum_{n=1}^{\infty} A_n \left[\begin{Bmatrix} \cos\left(\frac{u_n}{a}x\right) + \frac{B_i}{u_n} \\ \sin\left(\frac{u_n}{a}x\right) \end{Bmatrix} \exp\left(-\frac{u_n^2}{a^2}\kappa t\right) x \int_{-\infty}^{\infty} B_y(v)\cos(vy)\exp(-v^2\kappa t)dv \right]$$

$$u_n : n-th\ root\ of\ \tan(u_n) = 2B_i u_n / (u_n^2 - B_i^2) \qquad (20)$$

When an instantaneous heat, Q_H (J/mm), is added in the region of $0 < x < 2\ell_3$ and $-b_w < y < b_w$ of an infinitely wide plate with thickness of a, at t = 0, then the initial condition is

$$\theta = Q_H / (4\rho c_p \ell_3 b_w),$$
$$0 < x < 2\ell_3;$$
$$-b_w < y < b_w$$
$$\theta = 0,\ the\ other\ region \qquad (21)$$

The initial condition of Equation 21 is separable like Equation 10, hence, A_n and $B_y(v)$ in Equation 20 can be determined from Equations 8a and 8b. When the depth of the instantaneous heat source, ℓ_3, becomes zero, the following equation is given from Equation 8:

$$\theta = \frac{Q_H}{a\rho c} \sum_{n=1}^{\infty} A_n \left[\begin{Bmatrix} \cos\left(\frac{u_n}{a}x\right) + \frac{B_i}{u_n} \\ \sin\left(\frac{u_n}{a}x\right) \end{Bmatrix} \exp\left(-\kappa t \frac{u_n^2}{a^2}\right) x \int_{-\infty}^{\infty} \frac{\sin(vb_w)\cos(vy)}{2\pi b_w v} \exp(-\kappa t v^2)dv \right] \qquad (22)$$

A solution for local preheating is obtained by integrating θ in Equation 22 with regard to t from t = 0 to t = τ. When q_h (J/mm²s) is the power of preheat added on the unit area, then $Q_H = 2b_w q_h dt$ and thus:

$$\theta = \frac{q_h}{\pi a \lambda} \sum_{n=1}^{\infty} A_n \left[\begin{Bmatrix} \cos\left(\frac{u_n}{a}x\right) + \frac{B_i}{u_n} \\ \sin\left(\frac{u_n}{a}x\right) \end{Bmatrix} \frac{\sin(vb_w)\cos(vy)}{v(u_n^2/a^2 + v^2)} x \int_{-\infty}^{\infty} \left[1 - \exp\left\{ -\kappa t \left(\frac{u_n^2}{a^2} + v^2 \right) \right\} \right] dv \right] \qquad (23)$$

where A_n is given in Equation 22.

Welding is, in general, started when temperature at the surface becomes a certain level of preheating temperature. Supposing τ_p is given as the time necessary for θ of Equation 22 to reach the required preheating temperature, then the termination of preheating can be regarded as the onset of an addition of another heat source with power of $-q_h$ at t = τ_p. Thus, the following equation gives the thermal history after the completion of preheating:

$$\theta = \theta(t) - \theta(t - \tau_p),$$
$$when\ t > \tau_p \qquad (24)$$

Calculation for Models I, II and III

Application of Model I to High Heat Input Welding

Single pass submerged arc welding (SAW) with three electrodes in tandem is typical of high heat input welding. Figure 3A shows a macrophotograph of a SAW weld section made under conditions shown in Table 1. In order to simulate a thermal history and to predict a HAZ shape for large heat input welds as shown in Fig. 3A, the point heat source of Model I was arbitrarily distributed in a manner shown in Fig. 4A by comparing its distribution with the shape of the molten weld pool.

Figure 5A shows the comparison of the experiment with the weld shape predicted from the calculation of the heat conduction for distributed point heat sources. The thermal properties used are in Table 2. The contour lines of the weld interface, the line of the phase transformation from ferrite to full austenite, A_{c3}, and the subcritical (ferritic and austenitic) transformation line, A_{c1}, have been determined metallurgically, while the computed lines have been obtained by searching points whose peak temperatures are equal to the melting temperatures, A_{c3} and A_{c1}, respectively. These temperatures have been obtained from empirical formulas into which the chemical compositions of the welded steel have been substituted (Ref. 19). Figure 6A shows thermal histories at the weld midthickness, where the solid line is obtained by the computation of heat flow and the dotted line is obtained experimentally. Fairly good agreement between the experiment and the calculation is recognized from Figs. 5A and 6A.

Another typical high heat input process is electrogas welding (EGW). Contrary to SAW, the surface heat transfer in EGW is accelerated by copper shoes cooled by water. Model I can also analyze the heat flow of EGW by selecting proper thermal properties. As seen in Table 2, the surface heat transfer coefficient in EGW is much higher than that in SAW. Figure 3B shows a macrophotograph of an EGW weld section made in the welding condition shown in Table 1. Figures 5B and 6B show the comparison of the experimental results with the HAZ shape and the thermal history at midthickness calculated by the distributed point heat sources given in Fig. 4B. The weld interface, A_{c3} and A_{c1}, transformation lines were determined in the same manner as the SAW. The experiments and the calculation are also in fairly good agreement with EGW. Therefore, Equation 14, which is the solution of Model I, can simulate the HAZ shape and thermal history of high heat input welding by properly distributing the point heat sources and selecting thermal properties.

Application of Model I to the Prediction of $t_{8/5}$

The solution for Model I differs from Tanaka's solution (Ref. 3) in the possibility of an arbitrary selection of a point heat source location. Figure 7 shows the calculated thermal histories of SAW under the welding conditions in Table 1. As seen in Fig. 7, the location of the point heat source affects the thermal history. However, a cooling time between 800° and 500°C, $t_{8/5}$, which welding engineers often use to assess transformation phenomena of ferritic steels, does not differ. This implies that $t_{8/5}$ can be predicted from the heat flow of a surface point heat source. Figure 8 shows $t_{8/5}$s from computation and experiments of shielded metal arc welding (SMAW). The welding conditions are shown in Table 1. Since $t_{8/5}$ is less influenced by the preheating method than t_{100}, uniform preheating has been assumed in the calculation for Fig. 8. The following equation is a solution for heat conduction of a plate of finite thickness preheated to T_p without neglecting surface heat transfer (Ref. 20):

$$\theta = 2\left(T_p - T_\infty\right)\sum_{n=1}^{\infty} A_n \left[\begin{array}{l} \left\{ \begin{array}{l} cos\left(\frac{u_n}{a}x\right) + \\ \frac{B_i}{u_n} sin\left(\frac{u_n}{a}x\right) \end{array} \right\} \\ x \left[\begin{array}{l} \frac{sin(u_n)}{u_n} - \\ \frac{B_i\{cos(u_n)\}}{u_n} \end{array} \right] \\ exp\left(-\kappa t \frac{u_n^2}{a^2}\right) \end{array} \right] \quad (25)$$

where $A_n = \dfrac{u_n^2}{u_n^2 + B_i^2 + 2B_i}$

$t_{8/5}$ in Fig. 8 has been calculated by the linear combination of Equation 14 (heat flow by a moving point heat source) and Equation 25 (heat flow of preheating).

The values of thermal properties vary as temperature changes, but they cannot be changed in the analytical calculation in this study, unlike numerical analyses. Hence, effective thermal properties are desirable to be introduced to fit calculated results with experimental results. In the calculation of $t_{8/5}$, the values of thermal properties have been changed depending on welding heat input energy, E (kJ/mm), because of the difference in the retention time at high temperatures. The thermal conductance, λ (J/°C mm^{2}s), used in Model I is

$$\lambda = 0.02633 + 2.82 \times 10^{-4} \times \eta E \qquad (26)$$

And diffusivity, κ (mm^2/s), in Model I is

$$\kappa = 4.0 + 1.23 \times 10^{-2} \times \eta E \qquad (27)$$

where η is the thermal efficiency of welding. The values of α and η used in this calculation are shown in Table 2.

Application of Model II to the Prediction of t_{100} of the Test Piece

Model II is a problem of an instantaneous line heat source. This model is applicable to a uniformly preheated plate. The assumption of a line heat is not valid for the entire case. In fact, Model II is limited to analyzing welding cooling times of lower temperatures, such as t_{100}, for a small test piece. Figure 9 shows t_{100} calculated by Equation 15 along with Equation 17 (heat flow of line heat) and Equation 15 along with Equation 18 (heat flow of a uniformly preheated test piece). It is seen that t_{100} is influenced considerably by preheating temperature although t_{100} is almost the same at preheating temperatures over 150°C (302°F) even under different welding heat inputs. As seen in Table 2, the values of λ and κ used in the calculation of t_{100} have differed from those in the computation for the weld shape and $t_{8/5}$ because the temperature range of interest differs in the two cases.

Application of Model III to the Prediction of t_{100} in Wide Plate Welding

A welded plate, in actual welding, can be considered to be infinitely wide and long. When preheating is conducted locally, t_{100} is influenced by the preheating width and preheat power. Model III has been introduced to analyze heat conduction in actual welding with local preheating. Cooling times such as t_{100} can be calculated by the linear combination of Model I and Model III. Figure 10 shows t_{100} calculated under different preheating temperatures, which are assumed to be measured at the center of the preheated area, that is, point P in Fig. 1C. It is understood from Fig. 10 that the higher preheat power causes the shorter time in t_{100}. This is because the higher preheat power raises the surface temperature in a more concentrated region around point P while the surrounding area still remains cool. Thermal properties used in the computation for Fig. 10 are the same as those in Fig. 9.

It is seen in Fig. 10 that t_{100} differs

depending on preheat power, q_h (J/mm^{2}s), even though the same preheating temperatures are employed. This is caused by nonuniform distribution at the start of welding. Figure 11A and 11B shows temperature distribution in a plate preheated to 200°C (392°F) in the surface temperature at the center of a preheated zone with different preheat powers. As preheat power is higher, temperature at the surrounding area is seen to become lower, and shorter t_{100} results.

Preheat power, which is an important parameter for heat conduction of preheating in Equation 23, is difficult to directly measure. Figure 12 shows a temperature increase at the center calculated from Equation 23. This figure provides a chart to estimate preheat power, q_h, from the time period of preheating until its termination. For instance, 200 s is supposed to be required as the time necessary to attain a preheating temperature of 75°C (168°F) under the ambient temperature of 0°C (32°F). In this case, T is zero and $(Tp - T)/q_h$ is found to be 1500 from the chart, and thus q_h must be 0.05 J/mm^{2}s.

Conclusion

A comprehensive solution of heat flow in welding has been found. This has been developed to analyze the heat conduction of three models: a moving heat source inside the plate without neglecting surface heat transfer (Model I); an instantaneous line heat source (Model II); and local preheating (Model III). Using these models, it becomes possible to predict HAZ shapes, welding thermal histories and cooling times in welding. On the basis of comparison of the calculation with experiments, the following conclusions are drawn:

1) An expanded heat source encountered in high heat input welding is modified by the distributed point heat sources of Model I. The computation of heat conduction by the distributed heat sources satisfactorily predicts contours of fusion line and phase transformation lines as well as thermal histories in SAW and EGW with high heat input.

2) Welding cooling time, $t_{8/5}$, necessary for phase transformation and HAZ hardness can be predicted by a point heat source of Model I on the plate surface. In this case, the values of thermal properties used in the computation depend on the heat input employed.

3) Welding cooling time, t_{100}, for small test pieces can be predicted by Model II because the type of heat source has no effect on the cooling time to lower temperatures. The values of thermal properties used for t_{100} differ from those for $t_{8/5}$.

4) Welding cooling time, t_{100}, for wide plates is influenced by preheat power which affects temperature distribution at the start of welding. The preheat power can be found from a chart obtained by computation of Model III.

Appendix

T	temperature (°C)
T_∞	ambient temperature (°C)
T_p	preheat temperature (°C)
θ	temperature relative to ambient temperature ($= T - T_\infty$) (°C)
κ	thermal diffusivity (mm^2/s)
ρ	density (kg/mm^2)
c_p	specific heat (J/kg °C)
x, y, z	coordinates fixed to a plate (mm)
λ	thermal conductance (J/°C mm s) ($\lambda = \rho c_p \kappa$)
α	surface heat transfer coefficient (J/°C mm^2 s)
t	time (s)
a	thickness of plate (mm)
v_s	welding velocity (mm/s)
b	width of specimen in Model II (mm)
c	length of specimen in Model II (mm)
B_i	Biot modulus ($= a\alpha/\lambda$)
B_b	Biot modulus ($= b\alpha/\lambda$)
B_c	Biot modulus ($= c\alpha/\lambda$)
d	depth of heat source (mm)
K_0	0 order modified Bessel function of the second kind
r	$= \sqrt{y^2 + (z - v_s t)^2}$ (mm)
q	welding heat input in Model I (J/s)
q_h	power of preheat in Model III (J/mm^2 s)
Q	instantaneous heat source in Model I (J)
Q_L	instantaneous line heat source in Model II (J)
Q_H	instantaneous heat source of pre-heating in Model III (J/mm)
b_w	half width of preheating in Model III (mm)
τ_p	time period until termination of preheating (s)L half length of an instantaneous line heat source in Model II (mm)
ℓ_1	half edge length of an instantaneous heat source in Model I (mm)
ℓ_2	half edge length of an instantaneous line heat source in Model II (mm)
ℓ_3	half depth of preheated area in Model III (mm)
E	welding energy (kJ/mm)
η	thermal efficiency of welding
$t_{8/5}$	welding cooling time between 800° and 500°C (s)
t_{100}	welding cooling time from solidification to 100°C (s)

References

1. Rosenthal, D. 1941. Mathematical theory of heat distribution during welding and cutting. *Welding Journal* 21(5):220-s to 234-s.

2. Rosenthal, D. 1946. The theory of moving sources of heat and its application to metal treatments. *Trans. AIME* 43(l1):849–866.

3. Tanaka, S. 1943. A study on heat conduction of a moving heat source. *Journal Japan Welding Society* 13(9):347–359.

4. Wells, A. 1952. Heat flow in welding. *Welding Journal* 31(5):263-s to 267-s.

5. Grosh, R., and Trabant, E. 1956. Arc welding temperature. *Welding Journal* 35(8):396-s to 400-s.

6. Adams, C. M., Jr. 1958. Cooling rates and peak temperatures in fusion welding. *Welding Journal* 35(5):210-s to 215-s.

7. Christensen, N., Davies, V., and Gjermundsen, K. 1965. Distribution of temperatures in arc welding. *British Welding Journal* 12(2):54–75.

8. Nunes, A. C., Jr. 1983. An extended Rosenthal weld model. *Welding Journal* 62(6):165-s to 170-s.

9. Eagar, T., and Tsai, N. 1983. Temperature fields produced by traveling distributed heat sources. *Welding Journal* 62(12):346-s to 355-5.

10. Goldak, J., Chakravarti, A., and Bibby, M. 1984. A new finite element model for welding heat sources. *Metall. Trans.* 15B(2):299–305.

11. Davis, M., Kapadia, P., and Dowden, J. 1986. Modeling the fluid flow in laser beam welding. *Welding Journal* 65(7):167-s to 174-s.

12. Rykalin, N. H., and Beketov, A. I. 1967. Calculating the thermal cycle in the heat-affected zone from the two-dimensional outline of the molten pool. *Welding Production* 14(9):42–47.

13. Mazumder, J., and Steen, W. M. 1980. Heat transfer model for CW laser material processing. *Journal of Applied Physics* 51(2):941–947.

14. Ashby, M. F., and Easterling, K. E. 1982. A first report on diagrams for grain growth in welds. *Acta Metall.* 30(11):1969–1978.

15. Ion, J. C., Easterling, K. E., and Ashby, M. F. 1984. A second report on diagrams of microstructure and hardness for heat-affected zones in welds. *Acta. Metall.* 32(11):1949–1962.

16. Henwood, C., Bibby, M., Goldak, J., and Watt, D. 1988. Coupled transient heat transfer-microstructure weld computations (Part B). *Acta Metall.* 36(11):3037–3046.

17. Kasuya, T., and Yurioka, N. 1989. Analysis of three-dimensional heat conduction in welding by dispersed point heat sources. IIW Doc. IX-1554-89.

18. Terasaki, T., Akiyama, T., Ishimoto, K., and Mori, Y. 1988. Proposal of equations to estimate the cooling time, $t_{8/5}$, from 800°C to 500°C. *Quarterly Journal Japan Welding Society* 6(2):301–305.

19. Seyffarth, P. 1982. Ver Verlag Technik Berlin. *Schweib-ZTU-Schaubilder*, pp. 13.

20. Carslaw, H. S., and Jaeger, J. C. 1959. *Conduction of Heat in Solids*, Oxford University Press. pp. 114.